# UDE-Based Current Control Strategy for *LCCL*-Type Grid-Tied Inverters

Yongqiang Ye, *Senior Member, IEEE*, and Yongkang Xiong

***Abstract*—*LCL* filter is usually used as an interface between inverters and the grid. However, due to the characteristics of *LCL* filter and system uncertainties, it is complex to design a controller with proper parameters. In this paper, with *LCCL* filter, the order of the inverter control system can be reduced from third order to first order, and an uncertainty and disturbance estimator based control strategy for grid-tied inverters with *LCCL* filter is proposed. Specifically, the proposed control strategy consists of differential feedforward, proportional–integral controller, and grid voltage feedforward. Moreover, with one-sampling computation plus half-sampling pulse width modulation delays considered, a simple and clear tuning algorithm for the proposed control strategy is presented. Finally, the inverter system with the proposed control strategy is investigated, and the effectiveness is supported by the tuning and comparative experiments with a 2-kW inverter.**

***Index Terms*—Current control, inverter, *LCCL* filter, tuning algorithm, uncertainty and disturbance estimator (UDE).**

## I. Introduction

AS A NECESSARY part of generation system, grid-tied inverter plays a very important role in ensuring high-quality power injected into the power grid. To attenuate the high-frequency current harmonics caused by the pulse width modulation (PWM), an $LCL$ filter is usually used as an interface between an inverter and the grid. Compared with $L$ filter, $LCL$ filter has stronger suppression capability for high-frequency harmonic [1]. However, $LCL$ filter is a third-order system with a resonance peak, which requires a more complex injected grid current controller to maintain system stability and track a periodic signal [2].

$LCCL$ filter, an interesting topology of $LCL$ filter, is proposed by Shen *et al.* [3], [4]. In this topology, the order of the filter (the controlled part) can be degraded from third order to first order by splitting the capacitor of the $LCL$ filter into two parts and selecting reasonable parameters of $LCCL$. The controller for inverters with $LCCL$ filter is simple to design, and the filter holds the suppression capability for high-frequency harmonics. Although the controlled variable has changed from the injected grid current to the splitting capacitor current, the resonance peak still exists inside $LCCL$ filter. To suppress the resonance peak of $LCCL$, lots of methods are available, e.g., passive damping method [5], active damping method [6], multiple-state feedback method [7], etc. And the control of the injected grid current can be achieved by controlling the splitting capacitor current when the resonance peak suppression method of $LCCL$ is designed appropriately. For the injected grid current control, several strategies exist, such as proportional–integral (PI) control, proportional–resonant (PR) control, and repetitive control (RC) [8], etc. Based on the internal model principle, RC and PR controls can introduce an infinite gain at any specified frequency to eliminate steady-state error [9], [10], but the robustness of the controllers is always the short slab.

Relatively speaking, PI control is widely used in industrial applications because of its simple structure and easiness to implement, although it cannot achieve infinite gain. An effective approach to compensate the PI control performance and attenuate the effect of the grid voltage is grid voltage feedforward [11], [12]. Furthermore, the selection of controller parameters is also an issue in the design of PI control. A convenient and explicit controller design method for PI control is proposed in [13]. Based on an accurate system model and disturbance information, the controller parameters can be easily picked out. However, it is difficult to obtain accurate inverter and disturbance models. For example, the order of $LCCL$ filter cannot be degraded to first order precisely due to parameter uncertainties. Therefore, the study of alleviating the effect of uncertainties and disturbances is necessary.

For uncertainties and disturbances of system, a number of techniques have been proposed in the past decades, which comprise adaptive control [14], sliding mode control [15], disturbance observer based control [16], active disturbance rejection control [17], time delay control [18], and uncertainty and disturbance estimator (UDE) based control [19]. Among them, the UDE-based control has become a research hotspot because of its good tracking performance, uncertainty, and disturbance rejection ability in linear systems [20], [21]. However, to our best knowledge, there are few studies on UDE-based control of grid-tied inverters with $LCL$ filter so far because the full state of the dynamic system of $LCL$ should be available in UDE-based control strategy [22]. Compared with PI controller,

Manuscript received April 27, 2017; revised July 24, 2017 and August 27, 2017; accepted September 26, 2017. Date of publication October 9, 2017; date of current version January 16, 2018. This work was supported in part by the National Natural Science Foundation of China under Grant 61473145, in part by the Qinlan Project of Jiangsu Province, in part by the Six Talent Peaks Program of Jiangsu Province under Grant 2016-XNY-030, and in part by the Natural Science Foundation of Jiangsu Province under Grant BK20140836. *(Corresponding author: Yongqiang Ye.)*

The authors are with the College of Automation Engineering, Nanjing University of Aeronautics and Astronautics, Nanjing 211106, China (e-mail: melvinye@nuaa.edu.cn; yongkang_xiong@foxmail.com).

Color versions of one or more of the figures in this paper are available online at http://ieeexplore.ieee.org.

Digital Object Identifier 10.1109/TIE.2017.2760850

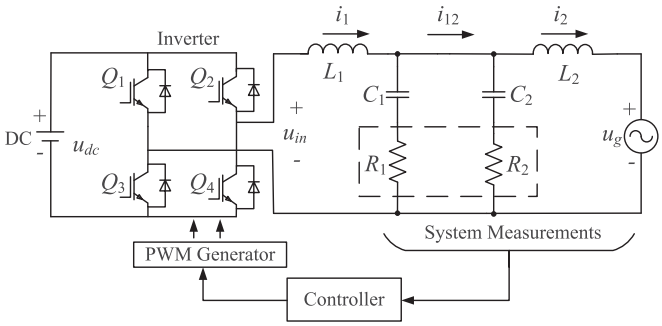


Fig. 1. System topology of the grid-tied inverter with $LCCL$ filter.

the cost of UDE-based controller will increase because it requires extra sensors. In this paper, based on $LCCL$ filter, the state variable of PI controller and UDE-based controller is the same. Therefore, the design of UDE-based controller for $LCCL$-type inverter is feasible.

In this paper, a UDE-based control strategy for grid-tied inverter with $LCCL$ filter is proposed, whose inverter topology is similar to that in [3], excepts that a group of passive damping resistances are added. According to the characteristics of the inverter, the design of the UDE-based controller is converted into the design of parameters $\alpha$, $\beta$, and $k$. A UDE-form PI controller is obtained by selecting proper UDE parameters. Unlike the traditional PI controller, the UDE-form PI controller parameters are determined by reference model parameters and low-pass filter parameters. With one-sampling computation plus half-sampling PWM delays considered, stability is analyzed and the range of the controller tuning knob $k$ is made clear. Aiming at engineering applications, a simple and clear tuning algorithm is provided. To attenuate the effect of the grid voltage, a feedforward method based on $LCCL$ is proposed. The effect of the delays on the grid voltage feedforward is discussed. It is revealed that the influence of the delays on the grid feedforward is negligible. Finally, tuning and comparative experiments are done on a 2-kW inverter.

The remainder of this paper is organized as follows. In Section II, the system structure and characteristics of $LCCL$ with passive damping resistance are demonstrated. In Section III, the UDE-based current controller is built and a design method for the parameters of UDE-based current control is studied. To suppress the injected grid current distortion arising from the grid voltage harmonics, a grid voltage feedforward method for inverter with $LCCL$ is proposed. In Section IV, experiments and remarks are given to validate the efficacy of the proposed scheme. Finally, the conclusion for this paper is provided in Section V.

## II. Model of $LCCL$ Filter

Fig. 1 shows the topology of a full-bridge single-phase grid-tied PWM inverter with $LCCL$ filter, where DC is the dc source, $u_{\rm dc}$ is the dc bus voltage, and $u_{\rm in}$ is the input voltage of the $LCCL$ filter that consists of inverter-side inductor $L_1$, grid-side inductor $L_2$, inverter-side capacitor $C_1$, and grid-side capacitor $C_2$. $R_1$ and $R_2$ in the dashed frame are a group of damping resistances. $i_1$ is the inductor current of $L_1$, $i_{12}$ is the current between $C_1$ and $C_2$, $i_2$ is the inductor current of $L_2$ (or called the injected grid current), and $u_g$ is the voltage of the grid. Different from the conventional current control scheme, the proposed control strategy for $LCCL$ is an indirect control method, where the controlled current is $i_{12}$ instead of $i_2$.

As proposed in [3], when the parameters satisfy the condition: $L_1+L_2=L$, $C_1+C_2=C$, $L_1=\gamma L$, $C_2=\gamma C$, neglecting $R_1$, $R_2$, and the equivalent series resistor of each component, the transfer function from $u_{\rm in}$ to $i_{12}$ can be expressed as

$$\begin{aligned} G_{i_{12}-u_{\rm in}}(s) &= \frac{i_{12}(s)}{u_{\rm in}(s)} \\ &= \frac{\gamma(1-\gamma)LCs^2+1}{\gamma(1-\gamma)L^2Cs^3+Ls} \\ &= \frac{1}{Ls}. \end{aligned} \tag{1}$$

Equation (1) indicates that $G_{i_{12}-u_{\rm in}}(s)$ can be degraded from third order to first order, and the result is similar to that with a single $L$ filter. Therefore, the injected grid current control system can be easily optimized, as claimed in [3]. And $1/Ls$ is the open loop of the controllable part of the inverter system. The uncontrolled part of the system, from $i_{12}$ to $i_2$, can be easily calculated and expressed as follows:

$$G_{i_2-i_{12}}(s)=\frac{i_2(s)}{i_{12}(s)}=\frac{1}{C_2L_2s^2+1}. \tag{2}$$

Equation (2) is a transfer function with a resonance peak. In order to attenuate the effect of resonance, a passive damping resistance $R_2$ is designed to connect in series with $C_2$, which is shown in Fig. 1. And (2) can be rewritten as

$$G_{i_2-i_{12}}(s)=\frac{i_2(s)}{i_{12}(s)}=\frac{1+R_2C_2s}{C_2L_2s^2+R_2C_2s+1}. \tag{3}$$

Different from (2), the resonance peak does not exist in (3) when an appropriate $R_2$ is selected. Equation (3) is a transfer function of a second-order low-pass filter, which has unity steady-state gain without phase lag at power frequency. Therefore, the control of $i_2$ can be achieved by controlling $i_{12}$. Compared with $L$ filter, $LCCL$ filter has a stronger high-frequency attenuation ability. However, the order degradation feature will not be maintained if only $R_2$ is added, so a symmetrical $R_1$ should be designed to connect in series with $C_1$, which is also shown in Fig. 1, and (1) can be rewritten as

$$G_{i_{12}-u_{\rm in}}=\frac{Z_1s^4+Z_2s^3+Z_3s^2+Z_4s+1}{(Z_1s^4+Z_2s^3+Z_3s^2+Z_4s+1)Ls}=\frac{1}{Ls} \tag{4}$$

where

$$\begin{aligned} Z_1 &= {R_1}^2L_2{C_1}^2C_2 \\ Z_2 &= 2R_1L_2C_2C_1+{R_1}^2R_2{C_1}^2C_2 \\ Z_3 &= L_2C_2+{R_1}^2{C_1}^2+2R_1R_2C_1C_2 \\ Z_4 &= 2R_1C_1+R_2C_2. \end{aligned}$$

As indicated by (4), the transfer function $G_{i_2-i_{12}}(s)=1/Ls$ is still valid, when $R_1+R_2=R$ and $R_1=\gamma R$. For an accurate

first-order system, it is easy to design a PI controller. However, (1) cannot always be established because the system parameters are usually inaccurate. Thus, a UDE-based control strategy for grid-tied inverters with $LCCL$ filter is proposed.

## III. UDE-Based Current Control

### A. Formation of UDE-Based Current Controller

As the transfer function of $LCCL$ filter is (1), the nominal voltage equation of $LCCL$ filter can be derived as

$$u_{\text{in}}(t) = L\frac{di_{12}(t)}{dt}. \tag{5}$$

When the PWM inverter is with unity gain, the state equation of the grid-tied inverter with $LCCL$ filter can be expressed as follows:

$$\dot{x}(t) = ax(t) + bu(t) + fx(t) + d(t) \tag{6}$$

where $x(t) = i_{12}(t)$ is the state variable, $u(t)$ is the control input variable, $f$ is the unknown dynamic coefficient of the grid-tied inverter, $d(t)$ is the known and unknown disturbance variable, $a = 0$, and $b = 1/L$.

For inverters with $LCCL$ filter, a desired closed-loop reference model can be expressed as

$$\dot{x}_m(t) = a_m x_m(t) + b_m u_m(t) \tag{7}$$

where $x_m(t) = i_{12}^*(t)$ is the desired state variable, $u_m(t)$ is the desired control input, $a_m$ is the desired coefficient, and $b_m$ is the desired control coefficient.

The tracking error $e(t)$ between $x_m(t)$ and $x(t)$ can be expressed as

$$e(t) = x_m(t) - x(t). \tag{8}$$

The control objective is to ensure that $e(t)$ converges to zero. One available method is to make $e(t)$ satisfy the condition

$$\dot{e}(t) = (a_m + k)e(t) \tag{9}$$

where $k$ is the error feedback gain, and $(a_m + k) < 0$.

By combining (6)–(9), we can obtain

$$\begin{aligned} &a_m x_m(t) + b_m u_m(t) - bu(t) - fx(t) - d(t) \\ &\quad = (a_m + k)e(t). \end{aligned} \tag{10}$$

Then, the control law can be derived as

$$u(t) = b^{-1}\left[a_m x(t) + b_m u_m(t) - fx(t) - d(t) - ke(t)\right] \tag{11}$$

where $b^{-1}$ is the inverse of $b$, $fx(t)$ and $d(t)$ can be unified into $u_d(t)$, which can be represented as

$$fx(t) + d(t) = u_d(t). \tag{12}$$

And according to (6), $u_d(t)$ can be expressed as

$$u_d(t) = \dot{x}(t) - bu(t). \tag{13}$$

Equation (13) indicates that the uncertainty and disturbance of a system can be observed by its system state and control signal.

Following the procedure in [20], when a proper low-pass filter $g_f(t)$ is selected, $u_d(t)$ can be approximated by a UDE $u_{\text{de}}(t)$ as

$$u_{\text{de}}(t) = u_d(t) * g_f(t) \tag{14}$$

where $*$ is the convolution operator. Then, by substituting (12) into (11), replacing $u_d(t)$ with $u_{\text{de}}(t)$, and taking the Laplace transform, the control law in $s$-domain can be obtained as

$$u(s) = b^{-1}\left[a_m x(s) + b_m u_m(s) - u_{\text{de}}(s) - ke(s)\right]. \tag{15}$$

By substituting (13) into (14), and then taking the Laplace transform, we can have

$$u_{\text{de}}(s) = \left[sx(s) - bu(s)\right] g_f(s). \tag{16}$$

Combining (15) and (16), a UDE-based control law can be derived as

$$\begin{aligned} u(s) = b^{-1}\Big[&a_m x(s) + b_m u_m(s) - ke(s) \\ &- sg_f(s)x(s)\Big]\frac{1}{1 - g_f(s)}. \end{aligned} \tag{17}$$

A simpler control law form can be derived after substituting the Laplace transform of (8) into (17) and eliminating $x(s)$ as follows:

$$u(s) = b^{-1}\left[sx_m(s) + \frac{sg_f(s) - (a_m + k)}{1 - g_f(s)}e(s)\right]. \tag{18}$$

Equation (18) shows that the proposed control law is relevant to the reference model and low-pass filter $g_f(s)$. Hence, the design of the controller is transformed to the design of the reference model and $g_f(s)$.

To simplify the design of UDE-based control, the reference model can be choose as a first-order system, whose $a_m$ and $b_m$ can be set to $-\alpha$ and $\alpha$. Hence, the transfer function from $u_m(s)$ to $x_m(s)$ is $\alpha/(s + \alpha)$, where the bandwidth is $\alpha$. And the reference model is strictly stable if $\alpha > 0$.

The design principle of $g_f(s)$ is to ensure that it is a strictly proper low-pass filter that has unity steady-state gain and broad enough bandwidth [20]. However, an ideal filter is difficult to obtain for inverters, because the spectrum of disturbance caused by deadtime and control delay cannot be estimated accurately. Hence, a first-order low-pass filter is often selected, i.e., $g_f(s) = \beta/(s + \beta)$, where its bandwidth is $\beta$. And $\beta$ can be set to cover the spectrum of the major uncertainties and disturbances.

By substituting $a_m$ and $g_f(s)$ into (18), the ultimate form of the control law can be obtained as

$$u(s) = L \cdot \left\{sx_m(s) + \left[(\alpha + \beta - k) + \frac{(\alpha - k)\cdot\beta}{s}\right]\cdot e(s)\right\} \tag{19}$$

where $L$ is $b^{-1}$. Equation (19) shows that the control law consists of the differential of the reference state, and a conventional PI control law, shown in Fig. 2. Compared with the traditional PI control, $sx_m(s)$ can improve the dynamic performance of the system. And the control law only contains known variables and is independent of unknown dynamics and disturbances.

Furthermore, by substituting the Laplace transform of (12), the Laplace transform of (14), and (15) into the Laplace transform of (6), a two-degree-of-freedom structure of the system

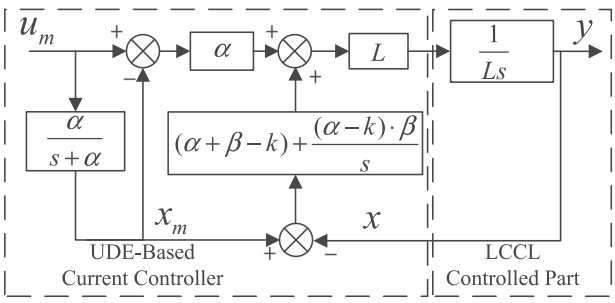


Fig. 2. Block diagram of the UDE-based control system.

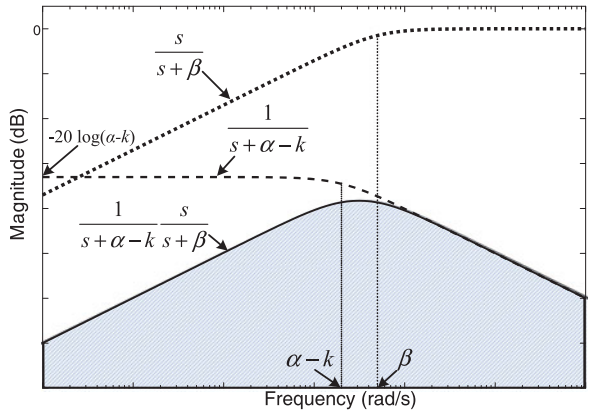


Fig. 3. Sketch of $u_d(s)$'s filter.

response can be obtained as

$$x(s) = \frac{b_m}{s-a_m}u_m(s) + \frac{1-g_f(s)}{s-a_m-k}u_d(s). \tag{20}$$

By substituting the proposed parameters, (20) can be expressed as

$$x(s) = \frac{\alpha}{s+\alpha}u_m(s) + \frac{1}{s+\alpha-k}\frac{s}{s+\beta}u_d(s). \tag{21}$$

Equation (21) indicates that the closed-loop transfer function is determined by the reference model and filtered $u_d(s)$, which means that the control law allows decoupling between reference tracking and disturbance rejection. In other words, the design of the error feedback gain and filter is decoupled in the frequency domain [19].

Fig. 3 is a sketch of the magnitude of $1/(s+\alpha-k)$, $s/(s+\beta)$, and their products.

As shown in Fig. 3, $u_d(s)$ can be attenuated by filter $1/(s+\alpha-k)$ and filter $s/(s+\beta)$, which means that the lumped disturbance $u_d(s)$ will be attenuated over the full bandwidth.

### B. $\alpha$, $\beta$, and $k$ Design

$\alpha$, $k$, and $\beta$ should be discussed before the tuning algorithm is given. According to Section III-A, $\alpha$ is the corner frequency of reference model $\alpha/(s+\alpha)$, $\alpha-k$ is the desired error convergence rate, and $\beta$ is the bandwidth of low-pass filter $\beta/(s+\beta)$. Consequently, one basic principle is $\alpha>0$, $\beta>0$, and $\alpha-k\geq 0$.

The object of the proposed UDE-based control law is to make $x(s)$ track $x_m(s)$ with zero steady-state error, and the tracking error convergence rate increases with the increase of $\alpha-k$. As mentioned earlier, an ideal low-pass filter $g_f(s)$ should cover the spectrum of $u_d(s)$, and the disturbance restrain capacity will be stronger with the increase of $\beta$. Hence, $\beta$ and $\alpha-k$ should be large enough, and with the increase of $\beta$ and $\alpha-k$, the performance of UDE-based controller becomes better.

However, according to (19), the PI parameters can be expressed as: $k_p=(\alpha-k+\beta)$ and $k_i=(\alpha-k)\cdot\beta$. Too large $\beta$ or $\alpha-k$ will cause instability. Therefore, $\alpha$, $k$, and $\beta$ are limited.

Above all, $\alpha$, $k$, and $\beta$ are in a trilaterally constrained relationship. And the design of UDE-based controller is converted to the adjustment of $\alpha$, $k$, and $\beta$. On the premise of that the system satisfies stability, $\alpha-k$ and $\beta$ should be as large as possible, which is the basic tuning principle. The tuning procedure will be complex and inefficient if there are no other constraints for $\alpha-k$ and $\beta$. Therefore, more constraints are provided as follows.

1) For $\alpha$: When $\alpha$ is unreasonable, $\alpha/(s+\alpha)$ will cause a large phase lag at 50 Hz, which will make the power factor (PF) fail to meet the requirement. Hence, PF can be regarded as a constraint condition for $\alpha$. The relationship between $\alpha$ and PF can be expressed as

$$\text{PF} = \frac{1}{\sqrt{1+(\text{THD})^2}}\cos\varphi \tag{22}$$

where $\varphi$ is the phase lag caused by $\alpha/(s+\alpha)$ and THD is the total harmonic distortion. And the relationship between $\alpha$ and $\varphi$ can be expressed as

$$\varphi = \arctan\frac{2\pi f}{\alpha} \tag{23}$$

where $f=50$ Hz. The combined formula of (22) and (23) can be expressed as

$$\text{PF} = \frac{1}{\sqrt{1+\text{THD}^2}}\cos\left(\arctan\frac{100\pi}{\alpha}\right). \tag{24}$$

It is reasonable and practical to set a lower bound of PF and upper bound of THD, and then we can derive $\alpha$ from (24). For this paper, THD $=10\%$ can be regarded as a reasonable THD ceiling, and an acceptable lower bound of power factor is PF $=0.9945$, and the corresponding $\alpha$ $=10\,000$ rad/s (this is the ideal case, and the actual PF is smaller than the ideal one because the delays will impose small additional phase lag on $\varphi$).

2) For $\beta$: As indicated in Sections III-A and III-B, $\beta$ should cover the frequency spectrum of $u_d$. However, an exact spectrum cannot be obtained due to deadtime and control delay. For inverters, the frequency spectrum of $u_d$ can be estimated by open-loop simulations, by which $\beta$ can also be estimated. And the simulated frequency spectrum of the $LCCL$ inverter used in this paper is up to the 15th-

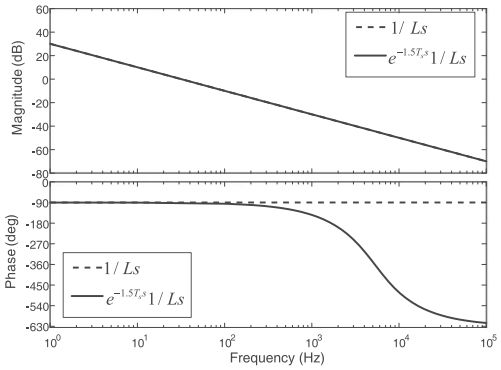


Fig. 4. Bode diagrams of $1/Ls$ and $e^{-1.5T_s s}1/Ls$.

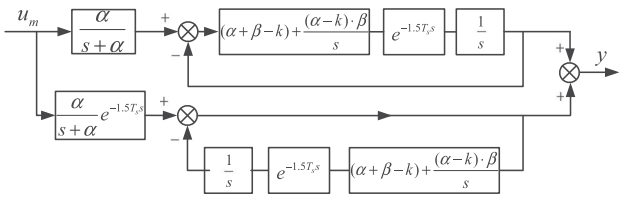

Fig. 5. Transformed block diagram of the UDE-based control system.

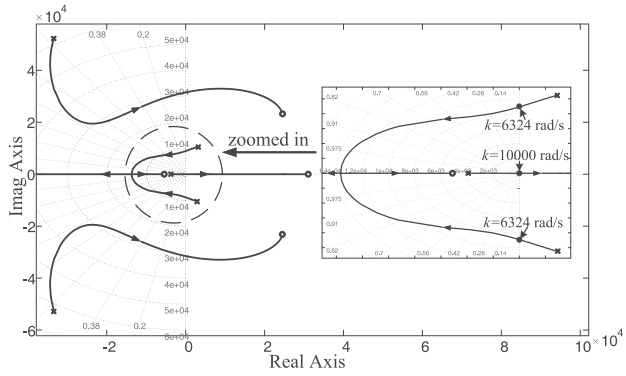


Fig. 6. Root locus with $\alpha = 10\,000$ rad/s, $\beta = 5000$ rad/s, and $k$ varying.

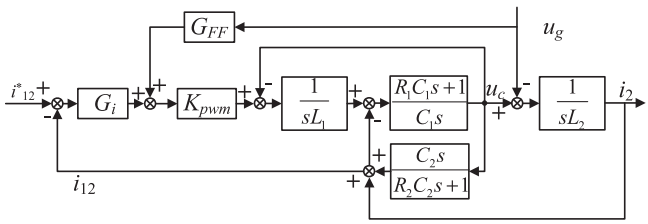

Fig. 7. Block diagram of the feedforward scheme.

order harmonic (i.e., 4710 rad/s), with which $\beta$ can be approximated as 5000 rad/s.

3) For $k$: In general, the error feedback gain $k$ may be set to zero when the reference model is stable [20]. But in this paper, $k$ is necessary because $\alpha - k$ is constrained, and $k$ can be regarded as the supplement of $\alpha$. In other words, $k$ increases the range of $\alpha$. Moreover, as mentioned above, after the control law is established and both $\alpha$ and $\beta$ are fixed, the stability of the system is determined by $k$. In digital control systems, there are one-sampling period computation delay and half-sampling period PWM delay [6], [23], the resulting PWM inverter gain and open-loop transfer function are $e^{-0.5T_s s}K_{\text{pwm}}$ and $e^{-1.5T_s s}1/Ls$ (when $K_{\text{pwm}} = 1$), respectively. The contrastive Bode diagrams of plant $1/Ls$ with and without $e^{-1.5T_s s}$ are shown in Fig. 4, where $e^{-1.5T_s s}$ is approximated by a third-order Pade approximation, which is precise enough because the conclusions drawn do not change as the order of Pade increases. Thus, the third-order Pade approximation is applied in all subsequent analyses. Fig. 4 shows that the delays have little effect on the magnitude of the plant, but a significant phase lag is introduced, which will influence the stability of the system. In this paper, $k$ is the only parameter that needs to be tuned after $\alpha$ and $\beta$ are fixed in the proposed parameters tuning algorithm, meaning that the range of $k$ is related to the stability of the system. To analyze the stability of the system, the block diagram in Fig. 2 is transformed with the delays considered, and the result is shown in Fig. 5. According to the closed-loop transfer function of the system in Fig. 5, the closed-loop characteristic equation can be derived as

$$1 - k\frac{s+\beta}{e^{1.5T_s s}s^2 + (\alpha+\beta)s + \alpha\beta} = 0. \qquad (25)$$

Then, the root locus of the closed-loop system is shown in Fig. 6 (in the case of $\alpha = 10\,000$ rad/s and $\beta = 5000$ rad/s), and the system is stable when 6324 rad/s $< k <$10 000 rad/s.

To summarize, $\alpha$, $k$, and $\beta$ design procedure can be described as following.

1) *Step 1:* Choose $\alpha = 10\,000$ rad/s and set initial $k = \alpha$.
2) *Step 2:* Select $\beta = 5000$ rad/s.
3) *Step 3:* Decrease and adjust $k$ from 10 000 to 6324 rad/s until the tracking performance is optimal.

According to the above-mentioned parameter tuning procedure, $\alpha$ and $\beta$ do not need to be designed precisely, because $k$ can play a good complementary role in the PI control law $L[(\alpha+\beta-k)+(\alpha-k)\beta/s]$, and only $k$ needs to be fine-tuned. This procedure is simpler and clearer, compared with PI tuning by trial and error.

As previously described, parameters $\alpha$, $\beta$, and $k$ of UDE-based control are limited, which means that the control gain cannot be infinite in the whole frequency band. Thus, the effect of power-grid harmonics is a nonignorable issue in the injected grid current controller design.

### C. Grid Voltage Feedforward

Full feedforward schemes of grid voltage can suppress the injected current distortion arising from the harmonics in grid voltage [11], [12].

Fig. 7 shows the control block of grid-tied inverter based on $LCCL$ with grid voltage full feedforward, where $G_i$ is the injected grid current controller, which is $L[(\alpha+\beta-k)+(\alpha-k)\beta/s]$ when $u_m = 0$, $G_{\text{FF}}$ is the transfer function of the grid voltage feedforward, the feedforward node is the output of $G_i$, $u_c$ is the series voltage of $C_1R_1$ ($C_2R_2$) branch,

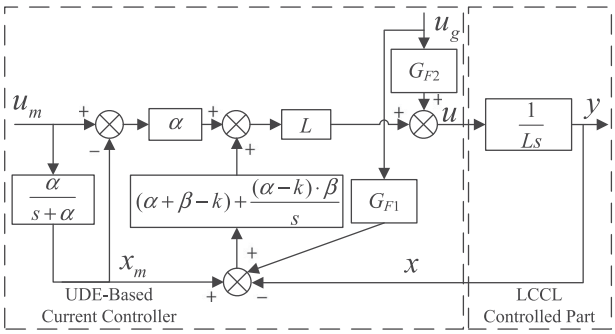


Fig. 8. Block diagram of UDE-based current control with feedforward.

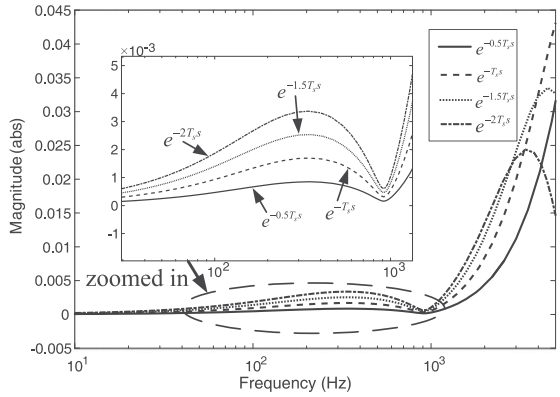


Fig. 9. Voltage full feedforward errors with different delays.

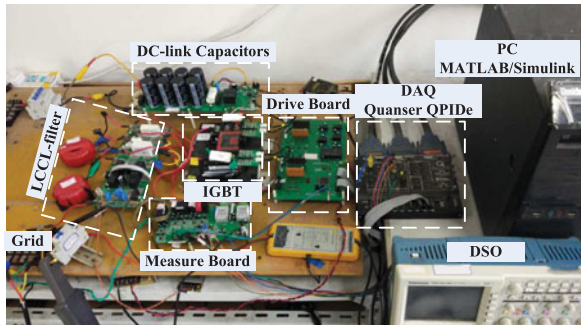


Fig. 10. Experimental setup.

and PWM inverter gain $K_{\text{pwm}} = 1$ that has been described in Section III-A.

According to the full feedforward schemes, to eliminate the effect of the $u_g$ on the injected current $i_2$, $u_c$ should be equal to $u_g$ when $i_{12}^* = 0$, and $G_{\text{FF}}$ can be derived as

$$G_{\text{FF}}(s) = 1 + \frac{G_i C_2 s}{1 + sC_2R_2} + \frac{L_1 s}{\gamma(1-\gamma)R + \frac{1}{Cs}} \tag{26}$$

where $\gamma(1-\gamma)R + 1/Cs$ is the parallel impedance of the two $CR$ branches. As indicated in (26), the second feedforward term $G_i C_2 s/(1 + sC_2R_2)$ contains controller $G_i$ so the feedforward node of the second feedforward term should move to the left of $G_i$. Then, the UDE-based controller with grid voltage feedforward can be represented by Fig. 8, where $G_{F1}$ is $C_2 s/(1 + sC_2R_2)$, and $G_{F2}$ is the sum of the first and third terms in (26).

In practice, the effect of the delays on the grid voltage feedforward should also be analyzed before it is applied. In the preceding part of this section, the derivation procedure of grid voltage feedforward is based on $K_{\text{pwm}} = 1$, and the resulting $G_{\text{FF}}$ does not contain delays. After one-sampling computation plus half-sampling PWM delays are taken into account, $G_{\text{FF}}$ is converted to $G_{\text{FF}n}$ that can be expressed as

$$G_{\text{FF}n}(s) = \frac{1}{K_{\text{pwm}} e^{-1.5T_s s}} + \frac{G_i C_2 s}{1 + sC_2R_2} + \frac{1}{K_{\text{pwm}} e^{-1.5T_s s}} \frac{L_1 s}{\gamma(1-\gamma)R + \frac{1}{Cs}}. \tag{27}$$

However, $G_{\text{FF}n}(s)$ is noncausal, which cannot be implemented. Thus, we have to use $G_{\text{FF}}(s)$ instead of $G_{\text{FF}n}(s)$. In order to study the full feedforward error produced by using $G_{\text{FF}}(s)$ instead of $G_{\text{FF}n}(s)$, we can define the grid feedforward error as $E_{G_{\text{FF}}}(s)$ that can be expressed as

$$E_{G_{\text{FF}}}(s) = u_g - \frac{G_{\text{FF}}(s)}{G_{\text{FF}n}(s)} u_g \tag{28}$$

where $G_{\text{FF}}(s)/G_{\text{FF}n}(s)u_g = u_c$, which is shown in Fig. 7. Obviously, $E_{G_{\text{FF}}}(s) = 0$ when the delays are neglected. And the transfer function from $u_g$ to $E_{G_{\text{FF}}}(s)$ can be represented as

$$G_e(s) = \frac{E_{G_{\text{FF}}}(s)}{u_g}. \tag{29}$$

The Bode plots of $G_e(s)$ below the Nyquist frequency with different delays are presented in Fig. 9 (in the case of $\alpha =$ 10 000 rad/s, $\beta = 5000$ rad/s, and $k = 8000$ rad/s). As indicated by the figure, the delays have an influence on the grid feedforward, and with the increase of the delay time, the grid feedforward error gain becomes greater. But on the whole, the feedforward error gain is small enough, and the gain at 50 Hz is less than $1 \times 10^{-3}$. Thus, it is reasonable to use $G_{\text{FF}}(s)$ instead of $G_{\text{FF}n}(s)$ to implement grid voltage full feedforward.

## IV. Experimental Verifications

A 2-kW prototype is built to validate the efficacy of the proposed scheme, as shown in Fig. 1. The inverter consists of an insulated gate bipolar transistor inverter bridge, an $LCCL$ filter with damping resistances, one current sensor for $i_{12}$, and two voltage sensors for $u_{\text{dc}}$ and $u_g$. Besides, $i_2$ is independent of the control, which is only used to observe the characteristics of the injected grid current and can be monitored by an oscilloscope. The single-phase grid-tied inverter is controlled by a Quanser QPIDe card, which is connected with a PC running MATLAB/Simulink and QuanRC. The experimental setup is shown in Fig. 10 and the parameters of the inverter are listed in Table I. One can refer to [3]–[5] for detailed design principles of damping resistances.

Fig. 11 shows the result with the proposed current controller without voltage feedforward, in the case of $\alpha =$ 10 000 rad/s, $\beta = 5000$ rad/s, and $k = 8000$ rad/s. As illustrated in the figure,

TABLE I
EXPERIMENT PARAMETERS

| Parameter | Value | Parameter | Value |
|---|---|---|---|
| DC bus voltage $u_{dc}$ | 380 V | Inverter-side capacitor $C_1$ | 4 $\mu$F |
| Grid voltage $u_g$ | 220 V | Grid-side capacitor $C_2$ | 6 $\mu$F |
| Sampling period $T_s$ | 100 $\mu$s | Inverter-side resistance $R_1$ | 12 $\Omega$ |
| PWM frequency $f_c$ | 10 kHz | Grid-side resistance $R_2$ | 8 $\Omega$ |
| Inverter-side inductor $L_1$ | 3.8 mH | | |
| Grid-side inductor $L_2$ | 2.5 mH | | |

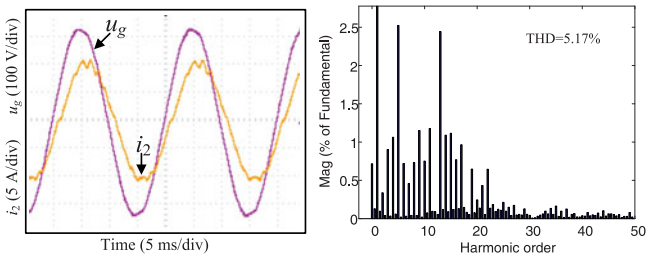


Fig. 11. Result of UDE-based control without grid voltage feedforward. (a) Injected grid current $i_2$. (b) Spectrum of the injected grid current.

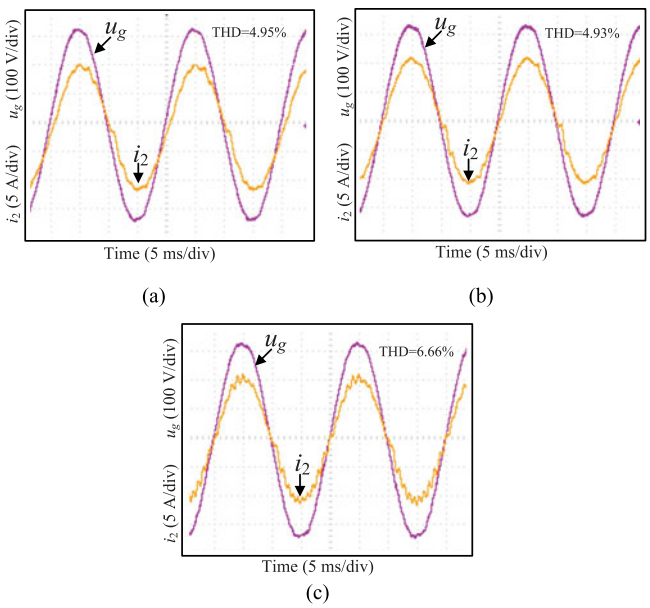


Fig. 12. Tuning results of UDE-based control with the same $\alpha$ = 10 000 rad/s, $\beta$ = 5000 rad/s, and different $k$. (a) $k$ = 10 000 rad/s. (b) $k$ = 9000 rad/s. (c) $k$ = 7000 rad/s.

the injected grid current is distorted and lags behind the grid voltage. Then, the grid voltage feedforward is used in all subsequent experiments.

## A. Tuning of $k$

To verify the proposed tuning algorithm, a series of tuning experimental results are shown in Fig. 12. According to Section III-B, the values of $\alpha$ and $\beta$ are set as 10 000 rad/s and 5000 rad/s, respectively. As the only parameter that needs

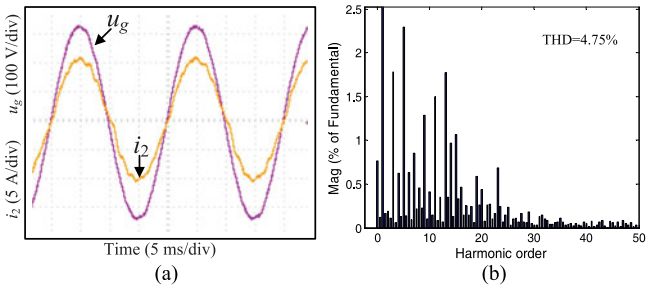


Fig. 13. Result of UDE-based control under $i_{12}^*(s)$ = 10 A with $\alpha$ = 10 000 rad/s, $\beta$ = 5000 rad/s, and $k$ = 8000 rad/s. (a) Injected grid current $i_2$. (b) Spectrum of the injected grid current.

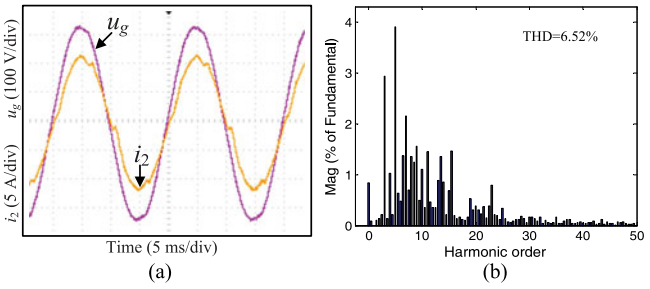


Fig. 14. Result of PI control under $i_{12}^*(s)$ = 10 A with $k_p$ = 17 and $k_i$ = 14400. (a) Injected grid current $i_2$. (b) Spectrum of the injected grid current.

to be tuned $k$ can be gradually decreased from the initial value 10 000 rad/s to the lower limit 6324 rad/s.

Fig. 12(a) indicates that the injected grid current cannot track the reference current despite that the current wave form is not badly distorted, and Fig. 12(b) denotes that the control performance becomes better when $k$ reduces. Nevertheless, when $k$ decreases too much, the system is unstable as shown in Fig. 12(c).

## B. Experimental Results

With the proposed tuning process, a set of optimal values can be eventually obtained, where $\alpha$ = 10 000 rad/s, $\beta$ = 5000 rad/s, and $k$ = 8000 rad/s. To compare with the traditional PI current controller with full feedforward of grid voltage, a set of comparative results are given in Figs. 13 and 14. And PI controller parameters $k_p$ and $k_i$ are optimal values decided by trial and error. Compared with PI, the proposed UDE-based control scheme performs well in terms of THD. Furthermore, comparing Figs. 11 and 13, it can be found that under the same control parameters, the grid voltage feedforward can significantly improve control performance, which means that the feedforward is necessary.

Fig. 15 shows that the injected grid current distortions decline with $i_{12}^*$ increasing, and the UDE-based control has obviously lesser distortion.

Furthermore, to analyze the robustness of the proposed control strategy, a set of experiments with parameters mismatching should be done. Without loss of generality, the experiments of changing $L$ have been chosen to verify the robustness of the proposed control strategy. According to (19), changing the value

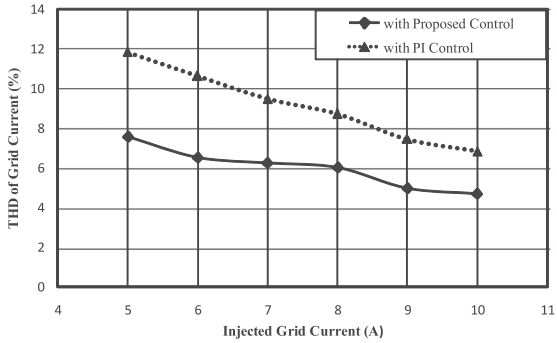


Fig. 15. THDs of the injected grid current with different $i_{12}^{*}$.

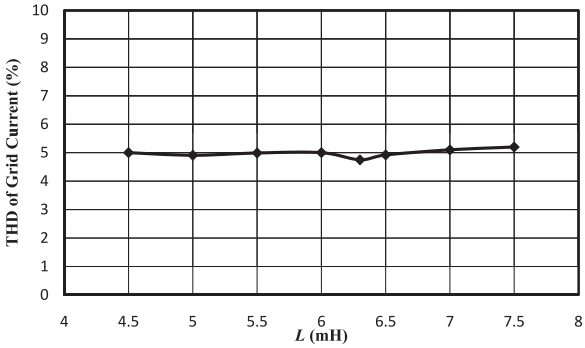


Fig. 16. THDs of the injected grid current with the variation of $L$.

of $L$ can be achieved by changing the value of $b^{-1}$ that is equal to the nominal value of $L$ (6.3 mH). Fig. 16 shows the trend with $L$ changing from 72% to 119% of the nominal value, implying that the proposed control strategy is robust to the inductance mismatching.

## V. Conclusion

For grid-tied inverter, $LCL$ filter is widely used to attenuate the high switching frequency harmonics caused by PWM. However, due to the characteristic of $LCL$ filter and uncertainty, it is complex to design a controller with proper parameters. In this paper, with $LCCL$ filter, the inverter control system can be degraded from third order to first order. And a UDE-based injected grid current control strategy was built. The proposed strategy unified the system uncertainty and disturbance into the lumped disturbances, and the closed-loop system adjusted by PI regulator approached to the reference model. Meanwhile, the PI controller can be expressed in the error feedback gain, the desired closed-loop bandwidth, and the approximate lumped disturbance bandwidth. Moreover, with one-sampling computation plus half-sampling PWM delays considered, a simple and clear tuning algorithm for the proposed control strategy was provided. Finally, the proposed strategy was verified by the tuning and comparative experiments on a 2-kW inverter.

## References

[1] M. Lindgren and J. Svensson, "Control of a voltage-source converter connected to the grid through an $LCL$-filter-application to active filtering," in *Proc. IEEE Power Electron. Spec. Conf.*, May 1998, pp. 229–235.

[2] E. Twining and D. G. Holmes, "Grid current regulation of a three-phase voltage source inverter with an $LCL$ input filter," *IEEE Trans. Power Electron.*, vol. 18, no. 3, pp. 888–895, May 2003.

[3] G. Shen, D. Xu, L. Cao, and X. Zhu, "An improved control strategy for grid-connected voltage source inverters with an $LCL$ filter," *IEEE Trans. Power Electron.*, vol. 23, no. 4, pp. 1899–1906, Jul. 2008.

[4] G. Shen, X. Zhu, J. Zhang, and D. Xu, "A new feedback method for PR current control of $LCL$-filter-based grid-connected inverter," *IEEE Trans. Ind. Electron.*, vol. 57, no. 6, pp. 2033–2041, Jun. 2010.

[5] R. P. Alzola, M. Liserre, F. Blaabjerg, R. Sebastián, J. Dannehl, and F. W. Fuchs, "Analysis of the passive damping losses in $LCL$-filter-based grid converters," *IEEE Trans. Power Electron.*, vol. 28, no. 6, pp. 2642–2646, Jun. 2013.

[6] D. Pan, X. Ruan, C. Bao, W. Li, and X. Wang, "Capacitor-current-feedback active damping with reduced computation delay for improving robustness of $LCL$-type grid-connected inverter," *IEEE Trans. Power Electron.*, vol. 29, no. 7, pp. 3414–3427, Jul. 2014.

[7] J. Dannehl, F. W. Fuchs, and P. B. Thogersen, "PI state space current control of grid-connected PWM converters with $LCL$ filters," *IEEE Trans. Power Electron.*, vol. 25, no. 9, pp. 2320–2330, Sep. 2010.

[8] Q. Zhao, Y. Ye, G. Xu, and M. Zhu, "Improved repetitive control scheme for grid-connected inverter with frequency adaptation," *IET Power Electron.*, vol. 9, no. 5, pp. 883–890, Apr. 2016.

[9] B. Zhang, D. Wang, K. Zhou, and Y. Wang, "Linear phase lead compensation repetitive control of a CVCF PWM inverter," *IEEE Trans. Ind. Electron.*, vol. 55, no. 4, pp. 1595–1602, Apr. 2008.

[10] R. Teodorescu, F. Blaabjerg, M. Liserre, and P. C. Loh, "Proportional-resonant controllers and filters for grid-connected voltage-source converters," in *Proc. Elect. Power Appl.*, vol. 153, no. 5, pp. 750–762, Sep. 2006.

[11] X. Wang, X. Ruan, S. Liu, and C. K. Tse, "Full feedforward of grid voltage for grid-connected inverter with $LCL$ filter to suppress current distortion due to grid voltage harmonics," *IEEE Trans. Power Electron.*, vol. 25, no. 12, pp. 3119–3127, Dec. 2010.

[12] W. Li, X. Ruan, D. Pan, and X. Wang, "Full-feedforward schemes of grid voltages for a three-phase $LCL$-type grid-connected inverter," *IEEE Trans. Ind. Electron.*, vol. 60, no. 6, pp. 2237–2250, Jun. 2013.

[13] C. Bao, X. Ruan, X. Wang, W. Li, D. Pan, and K. Weng, "Step-by-step controller design for $LCL$-type grid-connected inverter with capacitor-current-feedback active-damping," *IEEE Trans. Power Electron.*, vol. 29, no. 3, pp. 1239–1253, Mar. 2014.

[14] S. Tong, Y. Li, and S. Sui, "Adaptive fuzzy tracking control design for SISO uncertain nonstrict feedback nonlinear systems," *IEEE Trans. Fuzzy Syst.*, vol. 24, no. 6, pp. 1441–1454, Dec. 2016.

[15] N. Kumar, T. K. Saha, and J. Dey, "Sliding-mode control of PWM dual inverter-based grid-connected PV system: Modeling and performance analysis," *IEEE J. Emerg. Sel. Topics Power Electron.*, vol. 4, no. 2, pp. 435–444, Jun. 2016.

[16] E. Sariyildiz and K. Ohnishi, "Stability and robustness of disturbance-observer-based motion control systems," *IEEE Trans. Ind. Electron.*, vol. 62, no. 1, pp. 414–422, Jan. 2015.

[17] J. Han, "From PID to active disturbance rejection control," *IEEE Trans. Ind. Electron.*, vol. 56, no. 3, pp. 900–906, Mar. 2009.

[18] K. Youcef-Toumi and O. Ito, "A time delay controller for systems with unknown dynamics," *ASME J. Dyn. Syst. Meas. Control*, vol. 112, no. 1, pp. 133–142, 1990.

[19] B. Ren, Q.-C. Zhong, and J. Dai, "Asymptotic reference tracking and disturbance rejection of UDE-based robust control," *IEEE Trans. Ind. Electron.*, vol. 64, no. 4, pp. 3166–3176, Apr. 2017.

[20] Q.-C. Zhong and D. Rees, "Control of uncertain LTI systems based on an uncertainty and disturbance estimator," *J. Dyn. Syst. Meas. Control Trans.*, vol. 126, no. 4, pp. 905–910, Dec. 2004.

[21] J. Ren, Y. Ye, G. Xu, Q. Zhao, and M. Zhu, "Uncertainty-and-disturbance-estimator-based current control scheme for PMSM drives with a simple parameter tuning algorithm," *IEEE Trans. Power Electron.*, vol. 32, no. 7, pp. 5712–5722, Jul. 2017.

[22] Q.-C. Zhong, A. Kuperman, and R. K. Stobart, "Design of UDE-based controllers from their two-degree-of-freedom nature," *Int. J. Robust Nonlinear Control*, vol. 21, no. 17, pp. 1994–2008, 2011.

[23] D. Pan, X. Ruan, C. Bao, W. Li, and X. Wang, "Optimized controller design for $LCL$-type grid-connected inverter to achieve high robustness against grid-impedance variation," *IEEE Trans. Ind. Electron.*, vol. 62, no. 3, pp. 1537–1547, Mar. 2015.

**Yongqiang Ye** (M'06–SM'12) was born in Tongxiang, China. He received the B.E. and M.E. degrees from Zhejiang University, Hangzhou, China, in 1994 and 1997, respectively, and the Ph.D. degree from Nanyang Technological University, Singapore, in 2004, all in electrical engineering.

He was a Faculty Member of the School of Information, Zhejiang University of Finance and Economics, Hangzhou, China, for more than four years. He was also a Postdoctoral Research Fellow with the Department of Electrical Engineering, Lakehead University, Thunder Bay, ON, Canada, the Department of Systems and Computer Engineering, Carleton University, Ottawa, ON, Canada, and the Department of Mechanical Engineering, Dalhousie University, Halifax, NS, Canada, respectively. Since 2009, he has been a Professor in the College of Automation Engineering, Nanjing University of Aeronautics and Astronautics, Nanjing, China. He has authored or coauthored 1 book and more than 67 journal papers. His research interests include advanced control of power electronics and electrical machines.

**Yongkang Xiong** was born in Jiujiang, China. He received the B.E. degree in automation and M.E. degree in circuits and systems from East China University of Technology, Nanchang, China, in 2012 and 2015, respectively. He is currently working toward the Ph.D. degree in control theory and control engineering at Nanjing University of Aeronautics and Astronautics, Nanjing, China.

His research interests include power electronics control and disturbance rejection control technique.